# Electronic Supplementary Information

# Facile synthesis of intelligent nanocomposite as encapsulation for materials protection

*Peng Du, Juan Wang, Guangzhou Liu, Haichao Zhao* and Liping Wang**

P. Du, J. Wang, H. Zhao, L. Wang

Key Laboratory of Marine Materials and Related Technologies, Zhejiang Key Laboratory of Marine Materials and Protective Technologies, Ningbo Institute of Materials Technology and Engineering, Chinese Academy of Sciences, Ningbo 315201, China

P. Du, G. Liu

Institute of Marine Science and Technology, Shandong University, Qingdao 266200, China

**Table S1.** The composition of steel elements based on the EDS.

| Chemical element | Fe | Mn | Si | S | Cr | C | O |
|---|---|---|---|---|---|---|---|
| *w*/% | Bal. | 0.26 | 0.51 | 0.07 | 0.06 | 5.40 | 0.53 |

The carbon steel are composed of elements: Fe, Mn, Si, S, Cr, C and O.

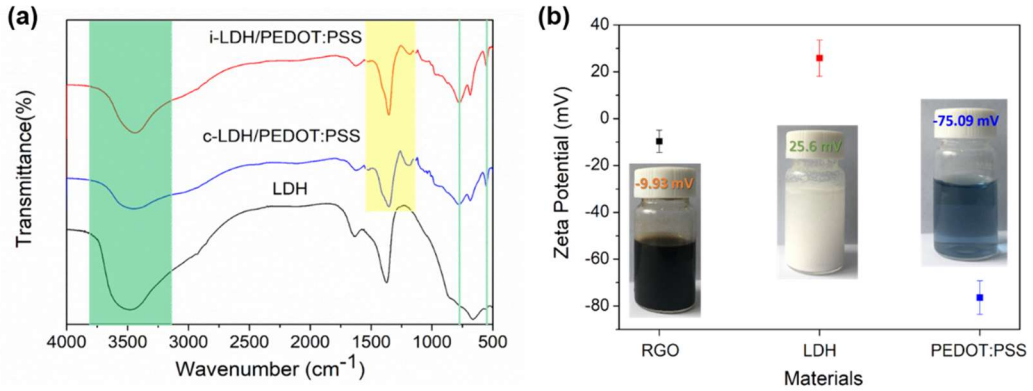


**Fig. S1** (a) FT-IR spectra of pristine LDH, i-LDH/PEDOT: PSS, and c-LDH/PEDOT: PSS; (b) ζ-Potential of RGO, LDH and PEDOT: PSS.

The above peaks indicate the presence of both PEDOT: PSS and LDHs components, which confirms that the PEDOT: PSS has intercalated in the galleries of LDHs successful modification. Because of the different value of ζ-Potential, RGO and LDH are excellent candidates for yielding the nanoplates structures with strong interfacial connections.

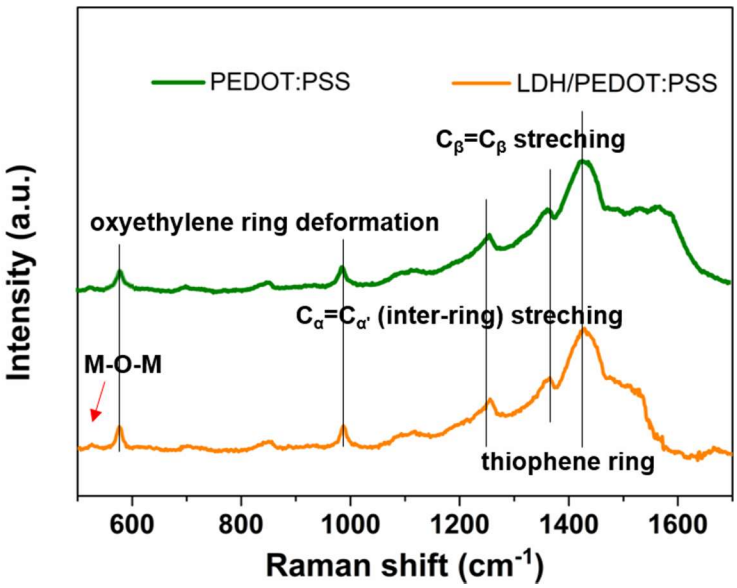


**Fig. S2** (a) Raman spectroscopy of PEDOT: PSS and c-LDH/PEDOT.

The extra peaks presented were the characteristic peaks of PEDOT: PSS/LDH, which were shown in Fig. S2. It confirms that, the PEDOT: PSS has been solidified by LDH.

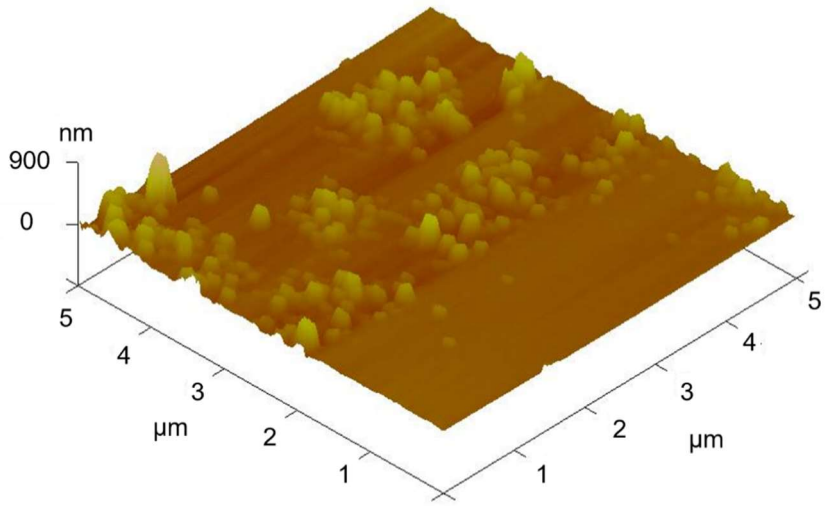


**Fig. S3** (a) AFM image (3D mode) of i-LDH/PEDOT:PSS@RGO.

As was shown in Fig. S3, the SPM tapping mode images exhibited the structure of i-LDH/PEDOT: PSS@RGO. The nanosheets were irregular in shape and the lateral size has lessened due to the damage during the ultrasonication assemble process.

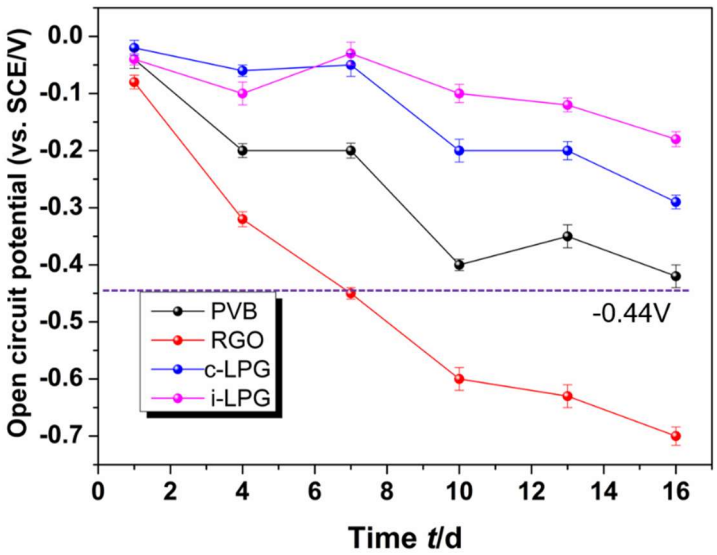


**Fig. S4** Open circuit potential for the samples.

Open circuit potential can be carried out to determine the protective effect of the coating systems. The changing potential means the increasing corrosion state. When it is under -0.44V (the corrosion potential of carbon steel), it means a severe corrosion process.

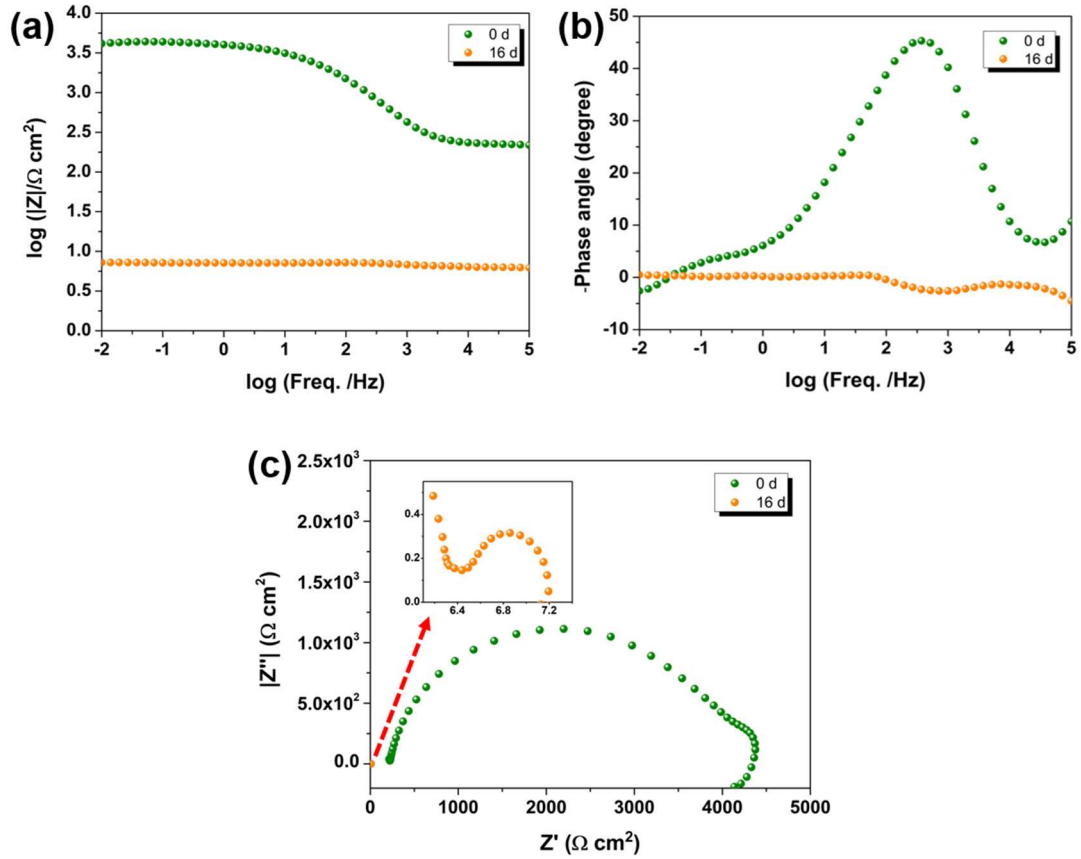


**Fig. S5** The Bode plots which show the impedance modulus and phase angle as a function of frequency logarithm (a, b) and the Nyquist plots of steel sheet (c).

As shown in Fig. S5, only one arc for the steel substrates exhibited in the plot of PS, which demonstrated that the sample has been corroded.

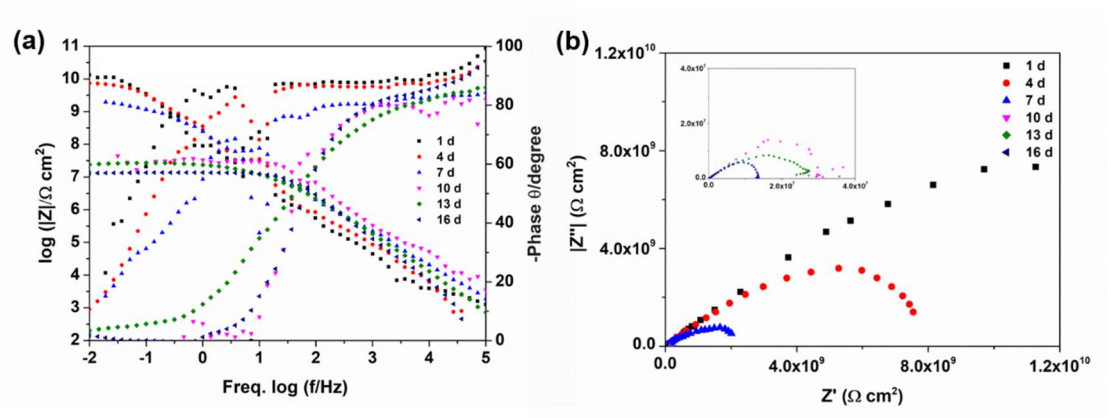


**Fig. S6** The Bode plots which show the impedance modulus and phase angle as a function of frequency logarithm (a) and the Nyquist plots of LDH/PEDOT: PSS (b).

The electrochemistry impedance characterization (CHI 660E, Shanghai Chenhua Ltd.) of the composite has demonstrated the corrosion-inhibitting and barrier function of the component-LDH/ PEDOT: PSS.

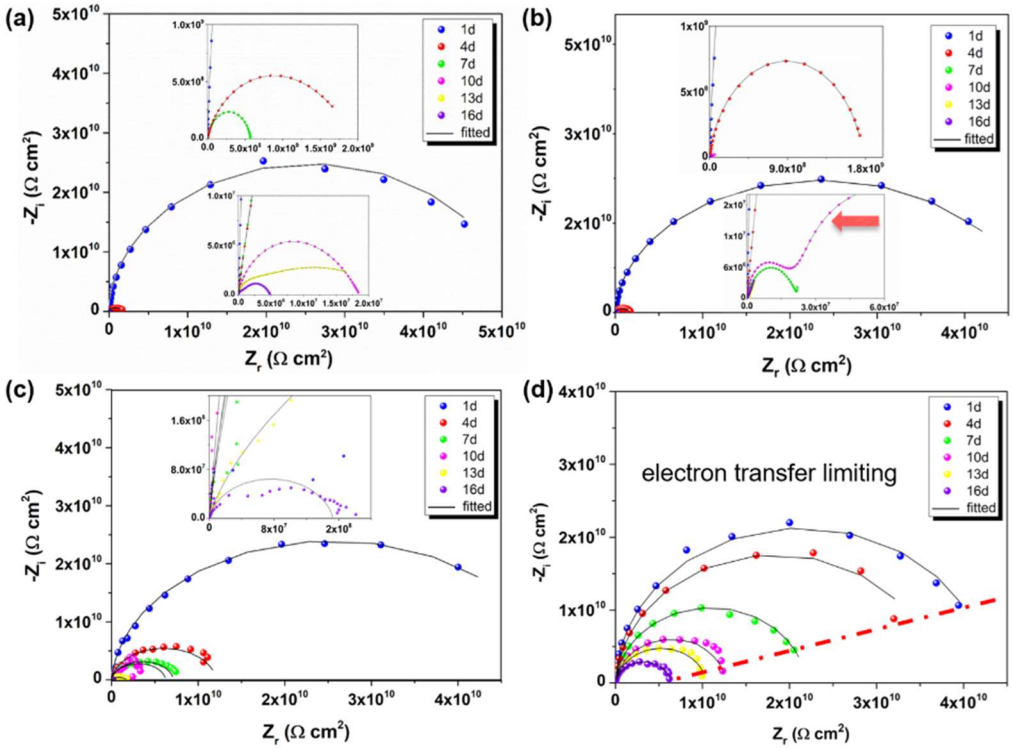


**Fig. S7** The Nyquist plots of the steel coated with PVB (a), RGO (b), i-LPG, (c) and c-LPG (d).

The fitting lines corresponding to EEC were exhibited in Fig. S7. It is generally known that radius could gradually become smaller as the immersion time went on. Compared with the uncoated steel sheets, the sample-PVB presented a capacitive arc at initial immersion time and then another radius also emerged at last. The trend of the curves indicated a gradual destruction process, which was attributed to the penetration of ions and barrier effect. Especially, observation of capacitive region of RGO after 10 days, two time constants presented, indicating the poor coating barrier performance of RGO nanosheets. It can be clearly known from the smaller capacitive arc (compared with PVB) at low frequency region, revealing the corrosion-acceleration, the RGO had harmful influence on its protection performance due to the galvanic corrosion.

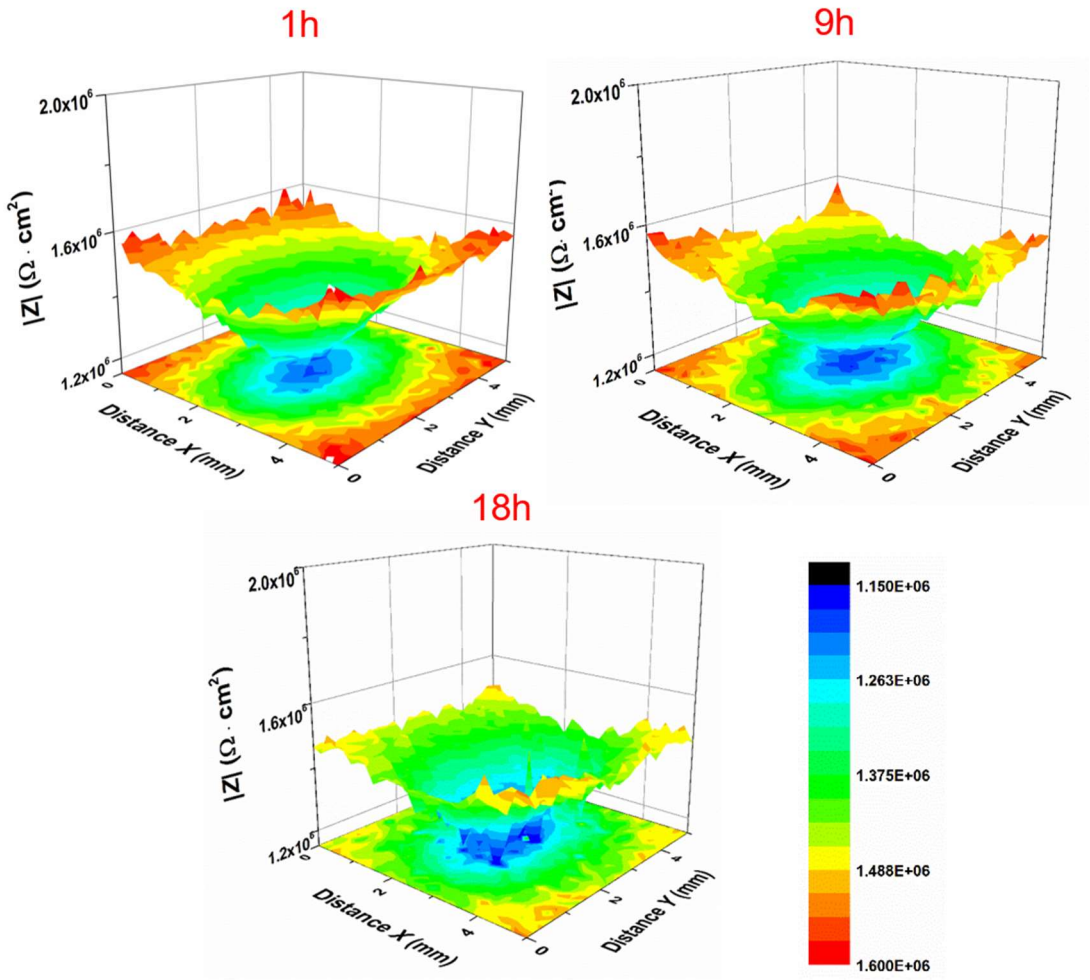


**Fig. S8** LEIS local impedance maps of i-LPG for immersion of 1 h, 9 h and 18 h.

The i-LPG reduced the micro-galvanic corrosion and showed significant physical barrier effect. To our surprise, in the case of the scratched i-LPG, corrosion behaviour obviously occurred in the damaged area after 9 hours' immersion owing to the oxygen has been consumed by the cathodic reaction. However, the extent of corrosion was much lower than that in the other specimens after 18 hours' immersion. Besides, the corrosion activity was suppressed by the coverage of the PEDOT: PSS film, as the corrosion current density declined.

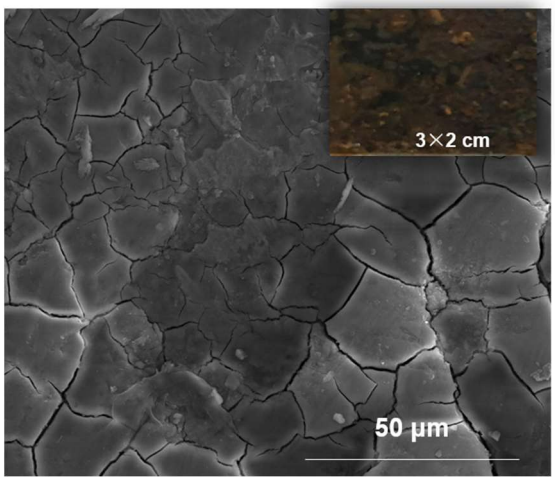


**Fig. S9** SEM images of the corroded steel sheets (inset: the digital photographs of the surface).

As illustrated in Fig. S9 and Table S1, loose porous corrosion product can be observed in the PS electrode. There are a large number of yellow rust layers and a few black rust layers existed in the digital image of PS, which are generated at the anode and cathode region, respectively. SEM images confirmed this conclusion due to the spherical goethite (α-FeOOH) and lump lepidocrocite (γ-FeOOH).

## Experimental section

Synthesis and exfoliation of graphene oxide

Graphene oxide was synthesized in a modified Hummers method. An appropriate amount of concentrated sulfuric acid was added to a 250 mL reaction flask in ice-water bath. Solid mixture of 2 g of graphite powder and 1 g of $NaNO_3$ was mixed in the flask and stirred until homogeneously suspended. Subsequently, 6 g of $KMnO_4$ was dispersed into the mixture, controlling the temperature below 20 ℃ under continuous stirring. The suspension was stirred at 35 ℃ for 30 min, and then a certain amount of deionized water was added after further stirring for additional 20 min. After adding an appropriate amount of $H_2O_2$, a brownish solution was presented.

The product was filtered when it was hot and then washed with 5% HCl solution and deionized water. Finally, the gel product was then diluted in water and exfoliated via ultrasonic treatment.

## Reference

(1) Yang, F.; Liu, T.; Li, J.; Qiu, S.; Zhao, H., Anticorrosive behavior of a zinc-rich epoxy coating containing sulfonated polyaniline in 3.5% NaCl solution. *RSC Advances* **2018,** *8* (24), 13237-13247.

(2) Kayser, L. V.; Russell, M. D.; Rodriquez, D.; Abuhamdieh, S. N.; Dhong, C.; Khan, S.; Stein, A. N.; Ramírez, J.; Lipomi, D. J., RAFT Polymerization of an Intrinsically Stretchable Water-Soluble Block Copolymer Scaffold for PEDOT. *Chemistry of Materials* **2018,** *30* (13), 4459-4468.

(3) Mazaheripour, A.; Majumdar, S.; Hanemann-Rawlings, D.; Thomas, E. M.; McGuiness, C.; d'Alencon, L.; Chabinyc, M. L.; Segalman, R. A., Tailoring the Seebeck Coefficient of PEDOT:PSS by Controlling Ion Stoichiometry in Ionic Liquid Additives. *Chemistry of Materials* **2018,** *30* (14), 4816-4822.

(4) Rao, C. N. R.; Sood, A. K.; Subrahmanyam, K. S.; Govindaraj, A., Graphene: The New Two-Dimensional Nanomaterial. *Angewandte Chemie International Edition* **2009,** *48* (42), 7752-7777.

(5) Dean, C. R.; Young, A. F.; Meric, I.; Lee, C.; Wang, L.; Sorgenfrei, S.; Watanabe, K.; Taniguchi, T.; Kim, P.; Shepard, K. L., Boron nitride substrates for high-quality graphene electronics. *Nature Nanotechnology* **2010,** *5* (10), 722-726.

(6) Qiu, S.; Li, W.; Zheng, W.; Zhao, H.; Wang, L., Synergistic Effect of Polypyrrole-Intercalated Graphene for Enhanced Corrosion Protection of Aqueous Coating in 3.5% NaCl Solution. *ACS Applied Materials & Interfaces* **2017,** *9* (39), 34294-34304.

(7) Arti, V.; Ajeet, K.; Atul, V.; Vidya, S.; Anujit, G.; K., G. Y.; Sharif, A.; Madhavan, N., Advances in Carbon Nanotubes–Hydrogel Hybrids in Nanomedicine for Therapeutics. *Advanced Healthcare Materials* **2018,** *7* (9), 1701213.

(8) Rasul, S.; Alazmi, A.; Jaouen, K.; Hedhili, M. N.; Costa, P. M. F. J., Rational design of reduced graphene oxide for superior performance of supercapacitor electrodes. *Carbon* **2017,** *111*, 774-781.